Journal of the Mechanics and Physics of Solids 122 (2019) 364–380

Contents lists available at ScienceDirect

Journal of the Mechanics and Physics of Solids

journal homepage: www.elsevier.com/locate/jmps

A simple explicit homogenization solution for the macroscopic elastic response of isotropic porous elastomers

Bhavesh Shrimali[a], Victor Lefèvre[b], Oscar Lopez-Pamies[a,*]

[a] Department of Civil and Environmental Engineering, University of Illinois at Urbana-Champaign, IL 61801, USA
[b] Department of Mechanical Engineering, Northwestern University, Evanston, IL 60208, USA

ARTICLE INFO

Article history:
Received 9 August 2018
Revised 4 September 2018
Accepted 21 September 2018
Available online 22 September 2018

Keywords:
Elastomers
Microstructures
Porosity
Constitutive modeling
Hamilton–Jacobi equations,

ABSTRACT

An approximate homogenization solution is put forth for the effective stored-energy function describing the macroscopic elastic response of isotropic porous elastomers comprised of incompressible non-Gaussian elastomers embedding equiaxed closed-cell vacuous pores. In spite of its generality, the solution — which is constructed in two successive steps by making use first of an iterative technique and then of a nonlinear comparison medium method — is fully explicit and remarkably simple. Its key theoretical and practical features are discussed in detail and its accuracy is demonstrated by means of direct comparisons with novel computational solutions for porous elastomers with four classes of physically relevant isotropic microstructures wherein the underlying pores are: (*i*) infinitely polydisperse in size and of abstract shape, (*ii*) finitely polydisperse in size and spherical in shape, (*iii*) monodisperse in size and spherical in shape, and (*iv*) monodisperse in size and of oblate spheroidal shape.

1. Introduction and main result

The prime objective of this paper is to construct an approximate homogenization solution for the effective stored-energy function describing the macroscopic elastic response of isotropic porous elastomers at arbitrary finite deformations.

Microscopic description of the porous elastomers of interest. More specifically, our focus in this work is on isotropic porous elastomers that comprise a statistically uniform and isotropic distribution of equiaxed — but of arbitrary shape otherwise — closed-cell vacuous pores embedded in an isotropic incompressible non-Gaussian elastomeric matrix. In its ground state, presumed to be undeformed and free of stress, the bounded domain in $\mathbb{R}^3$ occupied by any such porous elastomer is denoted by Ω_0 and its boundary by $\partial\Omega_0$. The largest characteristic size of the underlying pores is taken to be much smaller than the size of Ω_0 and, for convenience, units of length are chosen so that Ω_0 has unit volume. The constitutive behavior of the underlying elastomeric matrix is characterized by a free-energy density W_m, which is taken to be an objective and isotropic function of the deformation gradient tensor $\mathbf{F}$, in the sense that $W_m(\mathbf{QFK}) = W_m(\mathbf{F})$ for all $\mathbf{Q}, \mathbf{K} \in Orth^+$ and

* Corresponding author.
E-mail addresses: bshrima2@illinois.edu (B. Shrimali), victor.lefevre@northwestern.edu (V. Lefèvre), pamies@illinois.edu (O. Lopez-Pamies).

https://doi.org/10.1016/j.jmps.2018.09.026
0022-5096/

arbitrary **F**. In particular, we shall consider non-Gaussian free- or stored-energy functions of the form

$$W_{\rm m}(\mathbf{F}) = \begin{cases} \Psi_{\rm m}(I_1) & \text{if} \quad J = 1 \\ +\infty & \text{otherwise} \end{cases}, \tag{1}$$

where $I_1 = \mathbf{F}\cdot\mathbf{F} = F_{ij}F_{ij}$, $J = \det\mathbf{F}$, and where $\Psi_{\rm m}$ stands for any non-negative function of choice satisfying the linearization conditions[1] $\Psi_{\rm m}(3) = 0$ and $\Psi'_{\rm m}(3) = \mu/2$, with μ denoting the initial shear modulus of the elastomer, and the strong ellipticity conditions $\Psi'_{\rm m}(I_1) > 0$ and $\Psi'_{\rm m}(I_1) + 2(I_1 - \lambda_i^2 - 2\lambda_i^{-1})\Psi''_{\rm m}(I_1) > 0$ $(i = 1, 2, 3)$, with λ_1, λ_2, λ_3 denoting the singular values of **F**; see, e.g., Zee and Sternberg (1983). At any material point $\mathbf{X}\in\Omega_0$, it then follows that the first Piola–Kirchhoff stress tensor **S** is given by

$$\mathbf{S}(\mathbf{X}) = \frac{\partial W}{\partial \mathbf{F}}(\mathbf{X}, \mathbf{F}) \quad \text{with} \quad W(\mathbf{X}, \mathbf{F}) = [1 - \theta_0(\mathbf{X})]W_{\rm m}(\mathbf{F}), \tag{2}$$

where θ_0 is the characteristic function describing the spatial locations occupied by the pores in Ω_0, namely, θ_0 takes the value of 1 if the position vector **X** lies within a pore and zero otherwise.

The macroscopic response. Granted the statistically uniform distribution of the pores and their vanishingly small length scale with respect to the macroscopic length scale of Ω_0, the homogenized or macroscopic constitutive response of a given porous elastomer of interest is formally defined as the relation between the volume average of the first Piola–Kirchhoff stress $\overline{\mathbf{S}} \doteq \int_{\Omega_0}\mathbf{S}(\mathbf{X})\mathrm{d}\mathbf{X}$ and the volume average of the deformation gradient $\overline{\mathbf{F}} \doteq \int_{\Omega_0}\mathbf{F}(\mathbf{X})\mathrm{d}\mathbf{X}$ under affine boundary conditions on $\partial\Omega_0$ (Hill, 1972). It follows from standard arguments that such a relation can be expediently cast in the variational form

$$\overline{\mathbf{S}} = \frac{\partial \overline{W}}{\partial \overline{\mathbf{F}}}(\overline{\mathbf{F}}, f_0), \quad \text{where} \quad \overline{W}(\overline{\mathbf{F}}, f_0) = \min_{\mathbf{F}\in\mathcal{K}}\int_{\Omega_0} W(\mathbf{X}, \mathbf{F})\mathrm{d}\mathbf{X}, \tag{3}$$

the effective stored-energy function, represents physically the total elastic energy (per unit undeformed volume) stored in the porous elastomer. In the above expressions, $\mathcal{K}$ stands for a sufficiently large set of admissible deformation gradients **F** with prescribed volume average $\overline{\mathbf{F}}$ and we have included the initial volume fraction of pores, or initial porosity, $f_0 \doteq \int_{\Omega_0}\theta_0(\mathbf{X})\mathrm{d}\mathbf{X}$ as an explicit argument for later convenience. Granted further the geometric isotropy of the distribution of pores and the constitutive isotropy of the elastomeric matrix, it follows that the effective stored-energy function $\overline{W}$ defined by the variational problem $(3)_2$ is an isotropic stored-energy function of the macroscopic deformation gradient $\overline{\mathbf{F}}$ and, by the same token, that it admits the expedient representations

$$\overline{W}(\overline{\mathbf{F}}, f_0) = \overline{U}(\overline{\lambda}_1, \overline{\lambda}_2, \overline{\lambda}_3, f_0) = \overline{\Psi}(\bar{I}_1, \bar{I}_2, \bar{J}, f_0)$$

in terms of the singular values $\overline{\lambda}_1, \overline{\lambda}_2, \overline{\lambda}_3$ of $\overline{\mathbf{F}}$, i.e., the macroscopic principal stretches, and in terms of the standard macroscopic principal invariants

$$\bar{I}_1 = \overline{\mathbf{F}}\cdot\overline{\mathbf{F}}, \quad \bar{I}_2 = \frac{1}{2}\Big[\bar{I}_1^2 - (\overline{\mathbf{F}}^T\overline{\mathbf{F}})\cdot(\overline{\mathbf{F}}^T\overline{\mathbf{F}})\Big], \quad \bar{J} = \det\overline{\mathbf{F}}. \tag{4}$$

In this paper, we shall construct a *simple explicit approximate solution* for the effective stored-energy function $\overline{W}$. We do so in two steps. First, based on the rigorous solution originally introduced in Lopez-Pamies et al. (2011a,b) in the context of an analysis of cavitation instabilities, recast for our purposes here in Section 2, and the novel full-field simulations presented in Section 3 for porous elastomers with various classes of microstructures, we work out in Section 4 an approximate solution for $\overline{W}$ for the basic case of porous Gaussian or Neo-Hookean elastomers, that is, when $\Psi_{\rm m} = \mu/2[I_1 - 3]$. In Section 5, we put to use this approximation in the context of a nonlinear comparison medium method (Lopez-Pamies et al., 2013) to work out in turn the approximate solution for $\overline{W}$ for the general case of porous elastomers with any choice of (the finite branch of the) stored-energy function $\Psi_{\rm m}$ for the elastomeric matrix. For convenience, we record this main result here:

$$\begin{cases} \overline{W}(\overline{\mathbf{F}}, f_0) = (1 - f_0)\Psi_{\rm m}\Big(\dfrac{\mathcal{I}_1}{1 - f_0} + 3\Big) \quad \text{with} \\ \\ \mathcal{I}_1 = \dfrac{3(1 - f_0)}{3 + 2f_0}\big[\bar{I}_1 - 3\big] + \dfrac{3}{\bar{J}^{1/3}}\left[2\bar{J} - 1 - \dfrac{(1 - f_0)\bar{J}^{1/3}\Big(3\bar{J}^{-2/3} + 2f_0\Big)}{3 + 2f_0} - \dfrac{f_0^{1/3}\bar{J}^{1/3}\big(2\bar{J} + f_0 - 2\big)}{\big(\bar{J} - 1 + f_0\big)^{1/3}}\right]. \end{cases} \tag{5}$$

Section 5 includes as well a discussion of the key theoretical and practical features of the approximate homogenization solution (5). Finally, we devote Section 6 to illustrating the accuracy of the proposed solution (5) via direct comparisons with computational solutions for various types of porous elastomers and for various types of loading conditions.

[1] Throughout we make use of the standard notation $y'(x) = \mathrm{d}y(x)/\mathrm{d}x$.

At the close of this introduction, it is fitting to recall the handful of existing approximate solutions for $\overline{W}$ that have been proposed hitherto in the literature[2], together with their salient features. The earliest approximation appears to be that put forth by Ogden (1978), which applies only to isochoric deformations when $\det\bar{\mathbf{F}}=1$ and corresponds to a rigorous upper bound, the so-called Voigt bound. Later, Hashin (1985) presented an exact solution for porous elastomers with the so-called hollow sphere assemblage (HSA) microstructure[3] under isotropic deformations when $\bar{\mathbf{F}}=\bar{J}^{1/3}\mathbf{I}$. More recently, Danielsson et al. (2004), making use of a trial field due to Hou and Abeyaratne (1992), proposed an approximate solution applicable to arbitrary macroscopic deformation gradients $\bar{\mathbf{F}}$ that corresponds in fact to a generalization of both the Voigt bound and the Hashin solution, as it reduces to the former result for isochoric deformations and to the latter for porous elastomers with the HSA microstructure under hydrostatic loading. In a different direction, making use of a linear comparison medium method (Lopez-Pamies and Ponte Castañeda, 2007a, Lopez-Pamies and Ponte Castaneda (2007b)) constructed an approximate solution applicable to arbitrary macroscopic deformation gradients $\bar{\mathbf{F}}$ that is, in general, more accurate than the result of Danielsson et al. (2004). However, the approximate solution for $\overline{W}$ introduced in Lopez-Pamies and Ponte Castañeda (2007b) has two notable drawbacks. The first one is that it does not recover exactly the evolution of the porosity and as a result it becomes increasingly more inaccurate for deformations with a larger isotropic component and smaller initial porosities; see Section 4.4 in Lopez-Pamies and Ponte Castañeda (2007a). The second drawback is that the solution is not explicit, instead, its computation requires the numerical solution of a system of seven nonlinear algebraic equations. Partly because its construction is based on a *nonlinear* — as opposed to a *linear* — comparison medium, the result (5) is free of these drawbacks.

In terms of computational solutions for $\overline{W}$, similar to the analytical ones outlined above, there is only a few partial results available in the literature; see, e.g., the finite-element results in Danielsson et al. (2004) and Wang and Henann (2016). Accordingly, a second objective of this work is to provide a substantial set of accurate computational results for the macroscopic elastic response of isotropic porous elastomers with various types of microstructures and constitutive behaviors of the elastomeric matrix under a broad range of loading conditions.

2. An exact solution for porous Neo-Hookean elastomers with pores of infinitely polydisperse size and abstract shape

As part of an analysis of the phenomenon of elastic cavitation in rubber, by making combined use of various classes of iterative techniques (deBotton, 2005; Francfort and Murat, 1986; Idiart, 2008; Lopez-Pamies, 2010b, Lopez-Pamies et al. (2011a)) constructed an exact solution for the effective stored-energy function of a fairly large class of porous elastomers wherein the pores are infinitely polydisperse in size and of abstract shape. When specialized to the class of isotropic porous elastomers of interest in this work and, in particular, when the underlying elastomeric matrix is Neo-Hookean with

$$W_{\rm m}(\mathbf{F})=\begin{cases}\Psi_{\rm m}(I_1)=\dfrac{\mu}{2}[I_1-3] & \text{if}\quad J=1\\ +\infty & \text{otherwise}\end{cases}, \tag{6}$$

their result for the effective stored-energy function $\overline{W}(\bar{\mathbf{F}},f_0)$ is given implicitly by the viscosity solution of the Hamilton–Jacobi partial differential equation (PDE)

$$f_0\frac{\partial\overline{W}}{\partial f_0}-\overline{W}-\max_{\boldsymbol{\omega}(\boldsymbol{\xi})}\int_{|\boldsymbol{\xi}|=1}\frac{1}{4\pi}\left[\boldsymbol{\omega}\cdot\frac{\partial\overline{W}}{\partial\bar{\mathbf{F}}}\boldsymbol{\xi}-W_{\rm m}\big(\bar{\mathbf{F}}+\boldsymbol{\omega}\otimes\boldsymbol{\xi}\big)\right]{\rm d}\boldsymbol{\xi}=0 \tag{7}$$

subject to the initial condition

$$\overline{W}(\bar{\mathbf{F}},1)=0. \tag{8}$$

For later reference, we note that in terms of the macroscopic principal stretches $\bar{\lambda}_1$, $\bar{\lambda}_2$, $\bar{\lambda}_3$, the initial-value problem (7)–(8) with (6) takes the explicit form (Lopez-Pamies et al., 2011b)

$$\begin{aligned}&f_0\frac{\partial\overline{U}}{\partial f_0}-\overline{U}+\mu\mathcal{G}_0+\mathcal{G}_1\frac{\partial\overline{U}}{\partial\bar{\lambda}_1}+\mathcal{G}_2\frac{\partial\overline{U}}{\partial\bar{\lambda}_2}+\mathcal{G}_3\frac{\partial\overline{U}}{\partial\bar{\lambda}_3}+\frac{\mathcal{G}_4}{\mu}\left(\frac{\partial\overline{U}}{\partial\bar{\lambda}_1}\right)\left(\frac{\partial\overline{U}}{\partial\bar{\lambda}_2}\right)+\frac{\mathcal{G}_5}{\mu}\left(\frac{\partial\overline{U}}{\partial\bar{\lambda}_1}\right)\left(\frac{\partial\overline{U}}{\partial\bar{\lambda}_3}\right)\\&+\frac{\mathcal{G}_6}{\mu}\left(\frac{\partial\overline{U}}{\partial\bar{\lambda}_2}\right)\left(\frac{\partial\overline{U}}{\partial\bar{\lambda}_3}\right)+\frac{\mathcal{G}_7}{\mu}\left(\frac{\partial\overline{U}}{\partial\bar{\lambda}_1}\right)^2+\frac{\mathcal{G}_8}{\mu}\left(\frac{\partial\overline{U}}{\partial\bar{\lambda}_2}\right)^2+\frac{\mathcal{G}_9}{\mu}\left(\frac{\partial\overline{U}}{\partial\bar{\lambda}_3}\right)^2=0\end{aligned} \tag{9}$$

with

$$\overline{U}(\bar{\lambda}_1,\bar{\lambda}_2,\bar{\lambda}_3,1)=0, \tag{10}$$

[2] In contrast to the lack of solutions for $\overline{W}$ in $\mathbb{R}^3$, there are a plurality of exact and approximate analytical solutions, as well as computational solutions, in $\mathbb{R}^2$; see, e.g., Lopez-Pamies and Ponte Castañeda (2004); Michel et al. (2007); Moraleda et al. (2007), and Lopez-Pamies and Idiart (2009).

[3] More generally, for the case when the spheres are not hollow but rather filled with some other material, these microstructures are commonly referred to as coated sphere assemblages; see, e.g., Chapter 7 in the monograph by Milton (2002) and references therein.

where we recall that $\overline{U}(\bar{\lambda}_1, \bar{\lambda}_2, \bar{\lambda}_3, f_0) = \overline{W}(\bar{\mathbf{F}}, f_0)$ and where the coefficients $\mathcal{G}_0$ through $\mathcal{G}_9$ are the explicit functions of the stretches $\bar{\lambda}_1$, $\bar{\lambda}_2$, $\bar{\lambda}_3$ given by expressions (25) in the Appendix.

Despite its inherent nonlinearity, the viscosity solution of (7)–(8) with (6) for $\overline{W}$, or equivalently that of (9)–(10) for $\overline{U}$, can be spelled out in closed form in the asymptotic limits of small and infinitely large deformations, as well as for purely isochoric deformations. We devote Section 2.1 through Section 2.3 below to present these three partial solutions. More generally, for arbitrary finite deformations, the initial-value problem (7)–(8) with (6) does not seem to admit a closed-form solution. In Section 2.4, we present a sample of numerical solutions for it that are generated via a weighted essentially non-oscillatory (WENO) finite-difference scheme (Lefèvre et al., 2018).

2.1. The limit of small deformations

As announced above, in the limit of small deformations as $\bar{\mathbf{F}} \to \mathbf{I}$, the initial-value problem (7)–(8) with (6) can be solved in explicit form; see Appendix B in Lopez-Pamies et al. (2011a) for the relevant details. In terms of the macroscopic invariants (4), the solution can be expediently written in the asymptotic form

$$\overline{W}(\bar{\mathbf{F}}, f_0) = \frac{\widetilde{\mu}}{2}\big[\bar{I}_1 - 3\big] - \widetilde{\mu}\big(\bar{J} - 1\big) + \frac{1}{2}\left(\widetilde{\kappa} + \frac{\widetilde{\mu}}{3}\right)\big(\bar{J} - 1\big)^2 + o\big(||\bar{\mathbf{F}} - \mathbf{I}||^3\big), \tag{11}$$

where

$$\widetilde{\mu} = \frac{3(1 - f_0)}{3 + 2f_0}\mu \qquad \text{and} \qquad \widetilde{\kappa} = \frac{4(1 - f_0)}{3f_0}\mu. \tag{12}$$

We remark that the formulae (12) are nothing more than the classical Hashin–Shtrikman (HS) bounds for the shear and bulk moduli of an isotropic porous elastic material with incompressible matrix (Hashin and Shtrikman, 1963).

2.2. Isotropic deformations

Another special class of macroscopic deformations for which the Hamilton–Jacobi Eq. (7) with (6) subject to the initial condition (8) allows for an explicit solution is that of isotropic deformations when $\bar{\mathbf{F}} = \bar{J}^{1/3}\mathbf{I}$; see Appendix B in Lopez-Pamies et al. (2011b). The solution reads as

$$\overline{W}(\bar{J}^{1/3}\mathbf{I}, f_0) = \frac{3\mu}{2}\left[\frac{2\bar{J} - 1}{\bar{J}^{1/3}} - \frac{2\bar{J} + f_0 - 2}{(\bar{J} + f_0 - 1)^{1/3}} f_0^{1/3} - (1 - f_0)\right]. \tag{13}$$

Interestingly, in spite of corresponding to a solution for a different type of microstructure, the result (13) agrees identically with the result of Hashin (1985) for a porous Neo-Hookean elastomer with the HSA microstructure under hydrostatic loading; see Section 5 in Lopez-Pamies et al. (2011a) for a discussion of this notable agreement.

2.3. The limit of infinitely large deformations

Finally, the solution for the initial-value problem (7)–(8) with (6) can also be worked out in closed form in the limit of infinitely large "tensile" deformations as $||\bar{\mathbf{F}}|| \to \infty$. To that end, it suffices to consider the limits $\bar{\lambda}_1 \to \infty$, $\bar{\lambda}_1, \bar{\lambda}_2 \to \infty$, and $\bar{\lambda}_1$, $\bar{\lambda}_2$, $\bar{\lambda}_3 \to \infty$ in the initial-value problem (9)–(10) for the effective stored-energy function $\overline{U}$, instead of that for $\overline{W}$, and to exploit the symmetries $\overline{U}(\bar{\lambda}_1, \bar{\lambda}_2, \bar{\lambda}_3, f_0) = \overline{U}(\bar{\lambda}_2, \bar{\lambda}_1, \bar{\lambda}_3, f_0) = \overline{U}(\bar{\lambda}_3, \bar{\lambda}_2, \bar{\lambda}_1, f_0)$ (idem for the other permutations in $\bar{\lambda}_i$) due to isotropy. To leading order, the result can be written in the form

$$\overline{W}(\bar{\mathbf{F}}, f_0) = \frac{(1 - f_0)\mu}{2 + f_0}\bar{I}_1 + \frac{3(1 + f_0^{1/3})(1 - f_0^{1/3})^3\mu}{2 + f_0}\bar{J}^{-2/3}. \tag{14}$$

Akin to the representation (11) for small deformations, the representation (14) for infinitely large deformations is also linear in the first invariant $\bar{I}_1$, independent of the second invariant $\bar{I}_2$, nonlinear in the third invariant $\bar{J}$, and of the separable form $\overline{W} = \overline{W}_{\bar{I}_1}(\bar{I}_1, f_0) + \overline{W}_{\bar{J}}(\bar{J}, f_0)$.

2.4. Sample WENO solutions for arbitrary finite deformations

For arbitrary macroscopic deformation gradients $\bar{\mathbf{F}}$, the initial-value problem (7)–(8) with (6) needs to be solved numerically. In this Section, we present a representative set of numerical solutions computed by means of a new scheme recently devised for this class of PDEs. Full details of the scheme can be found in Lefèvre et al. (2018). Here, for completeness, we briefly point out that it involves a fifth-order Runge–Kutta scheme that integrates — from $f_0 = 1$ to the desired

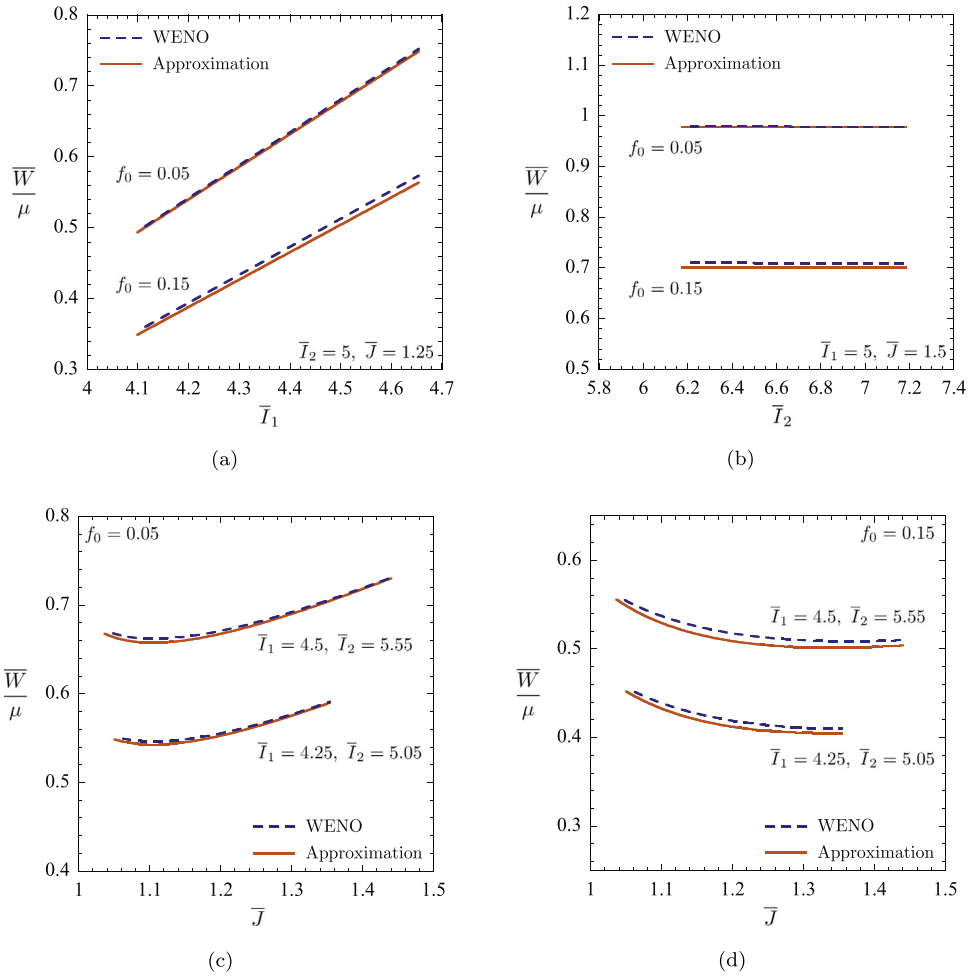

Fig. 1. The effective stored-energy function $\overline{W}$ defined by (7)–(8) with (6) for a porous Neo-Hookean elastomer with pores of infinitely polydisperse size and abstract shape plotted as a function of each of the three invariants $\bar{I}_1,\ \bar{I}_2,\ \bar{J}$ for fixed values of the remaining two invariants. The results are shown normalized with the initial shear modulus μ of the elastomeric matrix for two different initial porosities, $f_0 = 0.05$ and 0.15. The dashed lines (labeled "WENO") correspond to the numerical viscosity solution, while the solid lines (labeled "Approximation") correspond to the proposed explicit approximation (15).

value of the initial porosity $f_0 \in (0,\ 1)$ — the initial-value problem (9)–(10) for $\overline{U}$, wherein the partial derivatives with respect to $\bar{\lambda}_1,\ \bar{\lambda}_2,\ \bar{\lambda}_3$ are approximated via a fifth-order accurate WENO finite-difference scheme[4] The results that are reported below correspond to numerical solutions that were generated on the computational domains $x \doteq \ln(\bar{\lambda}_1/\bar{\lambda}_2) \in (0,\ 2.1)$, $y \doteq \ln(\bar{\lambda}_2/\bar{\lambda}_3) \in (0,\ 2.1)$, $z \doteq \ln(\bar{\lambda}_1\bar{\lambda}_2\bar{\lambda}_3) \in (-0.05, 2.1)$, $t \doteq -\ln f_0 \in (0, 3.0)$ for microstructures with initial porosity $f_0 = 0.05$, $x \in (0,\ 2.1)$, $y \in (0,\ 2.1)$, $z \in (-0.15, 2.1)$, $t \in (0,\ 1.9)$ for microstructures with $f_0 = 0.15$, and $x \in (0,\ 2.1)$, $y \in (0,\ 2.1)$, $z \in (-0.25, 2.1)$, $t \in (0,\ 1.4)$ for microstructures with $f_0 = 0.25$. Furthermore, all the results were generated on a fine Cartesian grid with spacings $h_x = 0.02, h_y = 0.04, h_z = 0.01$ for the finite-difference WENO approximations and with an increment $\Delta t = \min\{h_x, h_y, h_z\}/10 = 10^{-3}$ in the Runge–Kutta scheme. The relevant discretized equations were formulated and solved via a vectorized code written in the technical computing environment MATLAB (see MATLAB Version 8.3 Documentation, 2014b).

Now, for reasons that will become apparent further below, it proves helpful to plot the computed values of the effective energy $\overline{W}$, normalized by the shear modulus μ of the underlying Neo-Hookean matrix, as a function of each of the three invariants $\bar{I}_1,\ \bar{I}_2,\ \bar{J}$ while keeping the remaining two invariants fixed. Fig. 1 shows such plots for two representative cases of porous Neo-Hookean elastomers with initial porosities $f_0 = 0.05$ and 0.15. Part (a) of the figure shows $\overline{W}/\mu$ as a function of $\bar{I}_1$ for the pair of fixed values $\bar{I}_2 = 5$ and $\bar{J} = 1.25$ of the other two invariants. Similarly, part (b) shows $\overline{W}/\mu$ as a function of $\bar{I}_2$ for the pair of fixed values $\bar{I}_1 = 5,\ \bar{J} = 1.5$. Finally, parts (c) and (d) of the figure show $\overline{W}/\mu$ as a function of $\bar{J}$ for

[4] WENO schemes have the distinguishing attribute of enabling the discretized representation of the partial derivatives of a function with arbitrarily-high accuracy even when these exhibit discontinuities or steep gradients; see, e.g., the review of Shu (2009).

the pairs $\bar{I}_1 = 4.25,\ \bar{I}_2 = 5.05$ and $\bar{I}_1 = 4.5,\ \bar{I}_2 = 5.55$ for the initial porosity $f_0 = 0.05$ and $f_0 = 0.15,$ respectively. Here, it is important to remark that fixing the values of any pair of invariants $\bar{I}_1,\ \bar{I}_2,\ \bar{J}$ restricts the range of physically allowable values of the remaining invariant. The results displayed in Fig. 1 (as well as those displayed in Fig. 7 further below) pertain to the entire range of allowable values for each of the cases that is presented.

Three out of a total of four key observations from Fig. 1 are clearly that the effective stored-energy function $\overline{W}$ defined by (7)–(8) with (6) depends roughly linearly on the invariant $\bar{I}_1,$ nonlinearly on $\bar{J},$ and it is essentially independent of $\bar{I}_2$. Fig. 1(c) and (d) also serve to bring to the fore the fourth key observation: the effective stored-energy function remains, by and large, of the separable form $\overline{W} = \overline{W}_{\bar{I}_1}(\bar{I}_1, f_0) + \overline{W}_{\bar{J}}(\bar{J}, f_0)$ for arbitrary finite deformations; recall from (11) and (14) that $\overline{W}$ is exactly of this separable form in the limits of small and infinitely large deformations. A large set of results (beyond the illustrative ones presented here) has confirmed that such a distinctly simple functional dependence on the invariants $\bar{I}_1,$ $\bar{I}_2,$ and $\bar{J}$ holds true irrespectively of the value of initial porosity f_0 for the entire range $f_0 \in [0,\ 1]$; note that this class of infinitely polydisperse microstructures percolate at $f_0 = 1$.

3. Full-field solutions for porous Neo-Hookean elastomers with finitely polydisperse and monodisperse pores of spherical and non-spherical shape

The solution for $\overline{W}$ presented in the preceding section corresponds to, once more, a porous Neo-Hookean elastomer with pores that are of infinitely many sizes and of abstract shape. In this section, with the objective of gaining insight into the macroscopic effects of pore size dispersion and pore shape, we work out solutions for the effective stored-energy function $\overline{W}$ of porous Neo-Hookean elastomers with three other classes of microstructures: (*i*) an isotropic distribution of finitely polydisperse pores of spherical shape, (*ii*) an isotropic distribution of monodisperse pores of spherical shape, and (*iii*) an isotropic distribution of monodisperse pores of oblate spheroidal shape.

We begin in Section 3.1 through Section 3.3 by discussing the essential details of each of the three microstructures and proceed in Section 3.4 by providing an outline of the finite-element (FE) discretization employed to generate the numerical solutions for their effective stored-energy function $\overline{W}$. We devote Sections 3.5 and 3.6 to presenting a sample of such solutions at small and finite deformations.

3.1. Spherical pores of finitely polydisperse size

In order to computationally construct porous elastomers with an approximately isotropic distribution[5] of finitely polydisperse spherical pores, we model such materials as infinite media made out of the periodic repetition of a unit cell containing a random distribution of a large but *finite* number N of spherical pores featuring different sizes. By now, this approach has become a well-established technique to accurately yet efficiently approximate geometrically isotropic microstructures; see, e.g., Gusev (1997); Michel et al. (1999); Segurado and Llorca (2002), and Lopez-Pamies et al. (2013).

For definiteness, we select the defining unit cell to be a unit cube, with edges of length $L = 1,$ and consider that such a unit cell contains three families of spherical pores of different radii $R_{\rm p}^{(i)}$ and initial porosity $f_0^{(i)}$ $(i = 1, 2, 3)$ that are set to obey the following relations:

$$\left\{R_{\rm p}^{(1)}, R_{\rm p}^{(2)}, R_{\rm p}^{(3)}\right\} = \left\{R_{\rm p}, \frac{7}{9}R_{\rm p}, \frac{4}{9}R_{\rm p}\right\} \qquad \text{with} \qquad R_{\rm p} = L\left(\frac{3f_0^{(1)}}{4\pi N_{\rm p}}\right)^{1/3}$$

and

$$\left\{f_0^{(1)}, f_0^{(2)}, f_0^{(3)}\right\} = \{0.5f_0, 0.25f_0, 0.25f_0\} \qquad \text{with} \qquad f_0^{(1)} + f_0^{(2)} + f_0^{(3)} = f_0.$$

Here, $N_{\rm p}$ denotes the number of pores with the largest radius $R_{\rm p}^{(1)} = R_{\rm p}$ in the unit cell. We refer the interested reader to Section 5.2 in Lopez-Pamies et al. (2013) and Section 4.1 in Lefèvre and Lopez-Pamies (2017) for details of the construction of realizations with such microstructures via a random sequential adsorption algorithm[6] incorporating geometric constraints that allow for the eventual FE discretization of the resulting unit cells. For our purposes here, $N = 40$ pores turn out to be sufficient to achieve high degrees of isotropy. Accordingly, all results pertaining to polydisperse spherical pores that follow correspond to the case of $N_{\rm p} = 5,$ which leads to unit cells with a total of $N = 40$ pores. For illustration purposes, Fig. 2 shows examples of three such unit cells with initial porosities $f_0 = 0.05,$ 0.15, and 0.25.

[5] Note that an exactly isotropic distribution of pores — of spherical or any other shape — would involve infinitely many pores, which is, of course, computationally not feasible.

[6] Here, it is fitting to mention that random sequential adsorption algorithms can generate microstructures with pores of any size, shape, and orientation featuring porosities ranging from $f_0 = 0+$ to relatively close to their percolation limit, although reaching such high porosities could be computationally costly; see, e.g., Donev et al. (2004); Williams and Philipse (2003), and Anoukou et al. (2018). In this work, for each of the three classes of microstructures constructed with our random sequential adsorption algorithm, we have restricted attention to microstructures with porosities in the range $f_0 \in [0,\ 0.30]$, which are sufficiently away from their respective percolation limits. This is to avoid having to deal with the buckling of thin matrix ligaments between pores, which is beyond the scope of this work.

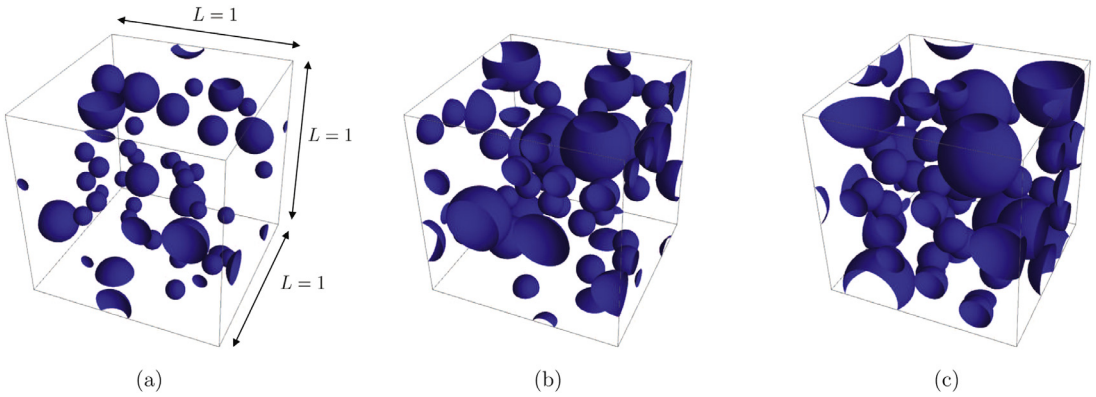

Fig. 2. Representative unit cells containing a random distribution of $N = 40$ spherical pores of three different sizes with three different initial porosities: (a) $f_0 = 0.05$, (b) $f_0 = 0.15$, and (c) $f_0 = 0.25$.

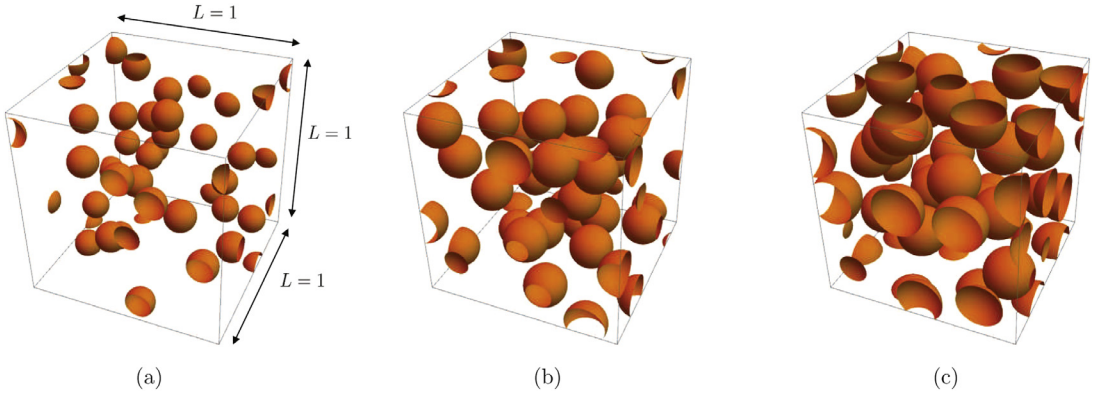

Fig. 3. Representative unit cells containing a random distribution of $N = 30$ spherical pores of the same size with three different initial porosities: (a) $f_0 = 0.05$, (b) $f_0 = 0.15$, and (c) $f_0 = 0.25$.

3.2. Spherical pores of monodisperse size

Porous elastomers with isotropic distributions of monodisperse spherical pores are modeled following the same preceding approach. For this class of microstructures, in terms of the number N of spherical pores of the same size and of the initial porosity f_0, it follows that the common radius of the pores is given by

$$R_{\mathrm{m}} = L\left(\frac{3f_0}{4\pi N}\right)^{1/3}.$$

The interested reader is referred to Section 5.1 in Lopez-Pamies et al. (2013) and Section 4.2 in Lefèvre and Lopez-Pamies (2017) for details of the construction of realizations with such microstructures. Based on a parametric study, unit cells with $N = 30$ pores lead to porous elastomers with elastic responses that are essentially isotropic. Accordingly, all results in this paper pertaining to monodisperse spherical pores correspond to unit cells with a total of $N = 30$ pores. Fig. 3 illustrates three such unit cells with initial porosities $f_0 = 0.05$, 0.15, and 0.25.

3.3. Oblate spheroidal pores of monodisperse size

To further probe the possible effects of the shape of the pores on the macroscopic response, we finally consider the case of porous elastomers wherein the pores are monodisperse in size and, for definiteness, oblate spheroidal in shape. Not to depart excessively from the focus of this work on pores that are equiaxed, we consider in particular the case of oblate spheroidal pores with moderate aspect ratio. The computational construction of this class of porous elastomers follows essentially the same procedure outlined above for those wherein the pores are spherical, with the addition that not only the center but also the orientation of each pore is randomly selected by the sequential adsorption algorithm. Chosen a number N of oblate spheroidal pores of the same size and of the same shape, their semi-diameters are given by

$$\{R_1, R_2, R_3\} = \{\omega R_{\mathrm{o}}, \omega R_{\mathrm{o}}, R_{\mathrm{o}}\} \qquad \text{with} \qquad R_{\mathrm{o}} = L\left(\frac{3f_0}{4\pi N\omega^2}\right)^{1/3}$$

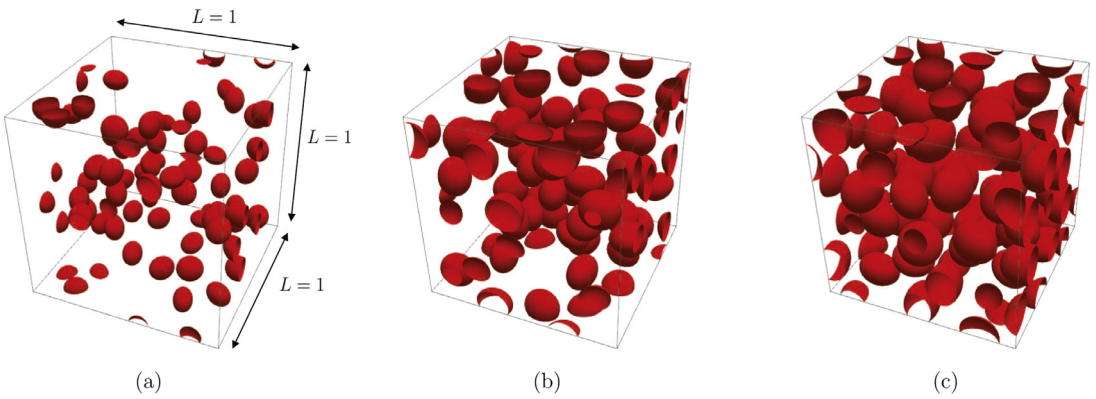

Fig. 4. Representative unit cells containing a random distribution of $N = 60$ oblate spheroidal pores of the same size and the same aspect ratio $\omega = 1.3$ with three different initial porosities: (a) $f_0 = 0.05$, (b) $f_0 = 0.15$, and (c) $f_0 = 0.25$.

in terms of the initial porosity f_0 and the desired ratio $\omega \geq 1$ of their equatorial radius $R_1 = R_2 = \omega R_o$ to their polar radius $R_3 = R_o$.

By way of an example, Fig. 4 shows representative unit cells with a total of $N = 60$ randomly distributed oblate spheroidal pores with aspect ratio $\omega = 1.3$ at three different initial porosities, $f_0 = 0.05, 0.15,$ and $f_0 = 0.25$. In the sequel, all results pertaining to monodisperse oblate spheroidal pores correspond to the case illustrated in this figure, namely, oblate spheroidal pores with the moderate aspect ratio of $\omega = 1.3$ and unit cells with $N = 60$ pores, which were checked to be sufficiently many in order to lead to elastic responses that are essentially isotropic.

3.4. Finite-element discretization

Having identified the porous elastomers with the microstructures of interest, we turn now to outlining the numerical computation of their effective stored-energy function $\overline{W}$. This is carried out via a hybrid FE scheme. In particular, we make use of a space discretization based on 10-node tetrahedral elements featuring approximations that are quadratic in the displacement field and linear in the pressure field; see, e.g., Chapter 8 in Boffi et al. (2013). We make use of the mesh generator code Netgen to create periodic FE discretizations of the unit cells (Schöbel, 1997). Discretizations with approximately 50,000 elements ($\sim$250, 000 degrees of freedom) were checked to produce sufficiently accurate results. Fig. 5 shows examples of such discretizations for each of the three microstructures defined above. The formulation of the relevant discretized equations and the computation of their solution were carried out in the commercial FE program ABAQUS making use of a user element subroutine; the C3D10H hybrid elements built in this program could also be readily used to generate the solutions (see ABAQUS Version 6.14 Documentation, 2014a).

As a final note in this section, we remark that all the FE results that are presented in the sequel correspond to the average of three realizations. For each type of porous elastomer considered, the responses of all three corresponding realizations showed very small differences (less than 2%) between one another.

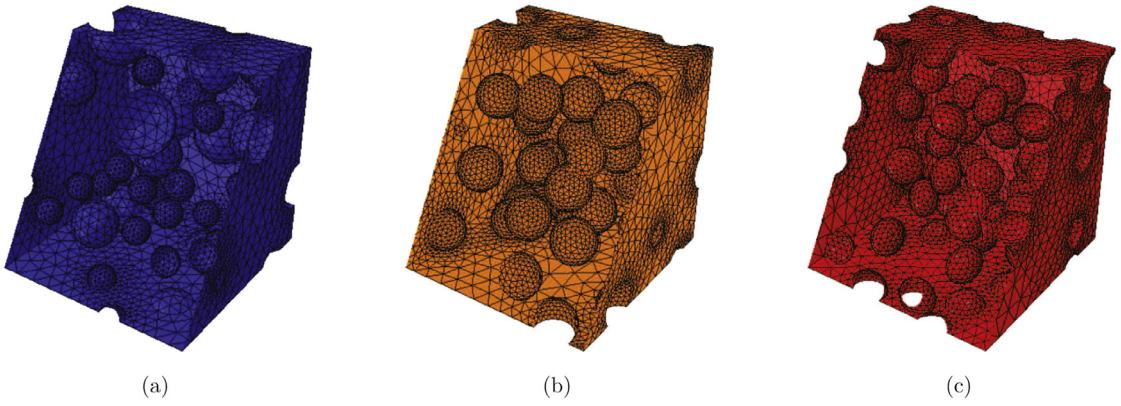

Fig. 5. Meshes in the undeformed configuration of representative unit cells for porous elastomers with initial porosity $f_0 = 0.15$ wherein the pores are: (a) polydisperse in size and spherical in shape, (b) monodisperse in size and spherical in shape, and (c) monodisperse in size and oblate spheroidal in shape.

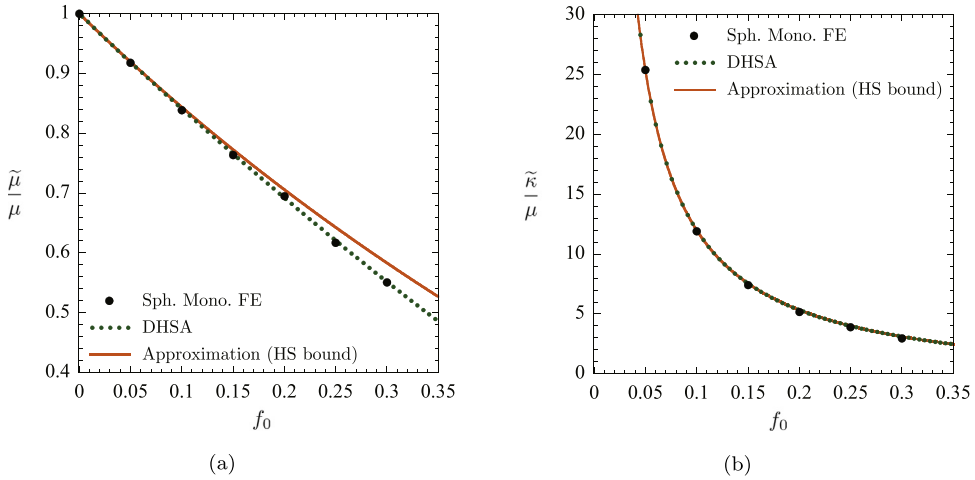

Fig. 6. FE solutions (solid circles) for the macroscopic elastic response in the limit of small deformations of a porous Neo-Hookean elastomer wherein the pores are monodisperse in size and spherical in shape. Parts (a) and (b) show, respectively, the normalized effective shear modulus $\widetilde{\mu}/\mu$ and the normalized effective bulk modulus $\widetilde{\kappa}/\mu$ as functions of the initial porosity f_0. For comparison purposes, the corresponding results for a differential hollow sphere assemblage (dotted lines) and the proposed explicit approximation (solid lines) are also included in the figure; as elaborated in Section 4, the latter are given by the HS bounds (12).

3.5. The limit of small deformations

Fig. 6 presents FE solutions for the macroscopic elastic response in the limit of small deformations of a porous Neo-Hookean elastomer with the isotropic distribution of monodisperse spherical pores described in Section 3.2; details of the FE calculations required in this asymptotic limit of small deformations can be found Appendix A of Spinelli et al. (2015). Specifically, plots are presented of the normalized values of the effective shear modulus $\widetilde{\mu}/\mu$ in Fig. 6(a) and of the effective bulk modulus $\widetilde{\kappa}/\mu$ in Fig. 6(b) as functions of the initial porosity f_0.

The corresponding results for the isotropic distributions of polydisperse spherical pores and monodisperse oblate spheroidal pores described in Sections 3.1 and 3.3 are virtually indistinguishable from those presented in Fig. 6 for monodisperse spherical pores, at least for all the initial porosities considered here, namely, from $f_0 = 0$ up to $f_0 = 0.30$. To further illustrate this insensitivity to pore size dispersion and pore shape, Fig. 6 includes for direct comparison the corresponding results for a porous elastomer with a differential hollow sphere assemblage (DHSA) microstructure[7], as well as the HS bounds (12), which, as elaborated above in Section 2.1, happen to correspond to the exact effective shear and bulk moduli of a porous Neo-Hookean elastomer with pores of infinitely polydisperse size and abstract shape. Thus, in view of these further comparisons, it is plain that neither the dispersion in size nor the shape of the pores have a significant effect — sufficiently away from percolation, of course — on the macroscopic elastic response of isotropic porous elastomers at small deformations. Instead, the comparisons point to the initial porosity f_0 as the *sole* microstructural quantity of significance.

3.6. Sample FE solutions for finite deformations

Fig. 7 presents FE solutions for the effective stored-energy function $\overline{W}$ of a porous Neo-Hookean elastomer with spherical pores of monodisperse size at finite deformations. Similar to the plots shown in Fig. 1, Fig. 7 shows the normalized energy $\overline{W}/\mu$ plotted in terms of each of the three invariants $\bar{I}_1$, $\bar{I}_2$, $\bar{J}$ for fixed values of the remaining two invariants. The results correspond to the same fixed values of the invariants and the same two initial porosities considered in Fig. 1.

Much like the results for small deformations presented in Fig. 6, the corresponding results for the isotropic distributions of finitely polydisperse spherical pores and monodisperse oblate spheroidal pores are indistinguishable from those presented in Fig. 7, again, for all the initial porosities considered here. Thus, even at finite deformations, the size dispersion and shape of the pores turn out to have little effect on the macroscopic elastic response of isotropic porous elastomers. Instead, rather remarkably, the initial porosity f_0 appears to be the sole microstructural quantity of significance, irrespectively of the applied deformation.

Another central observation from the results shown in Fig. 7 is that the effective stored-energy function $\overline{W}$ of porous Neo-Hookean elastomers with spherical (and oblate spheroidal) pores, much like that showcased in Fig. 1 for the porous

[7] We remind the reader that a DHSA is a HSA wherein hollow spheres of comparable size are placed far apart from each other and surrounded by hollow spheres of much smaller size; see, e.g., Avellaneda (1987) and Chapter 10.5 in the monograph by Milton (2002). While the effective bulk modulus of a DHSA agrees identically with the HS bound $(12)_2$, its effective shear modulus is given by the formula $\widetilde{\mu} = \mu - 70f_0\mu/(21 + 30f_0 + 19f_0^{10/3} + (361f_0^{20/3} + 76f_0^{13/3} - 5502f_0^{10/3} + 9408f_0^{8/3} - 4700f_0^2 - 84f_0 + 441)^{1/2})$; see Section III in Lefèvre and Lopez-Pamies (2014).

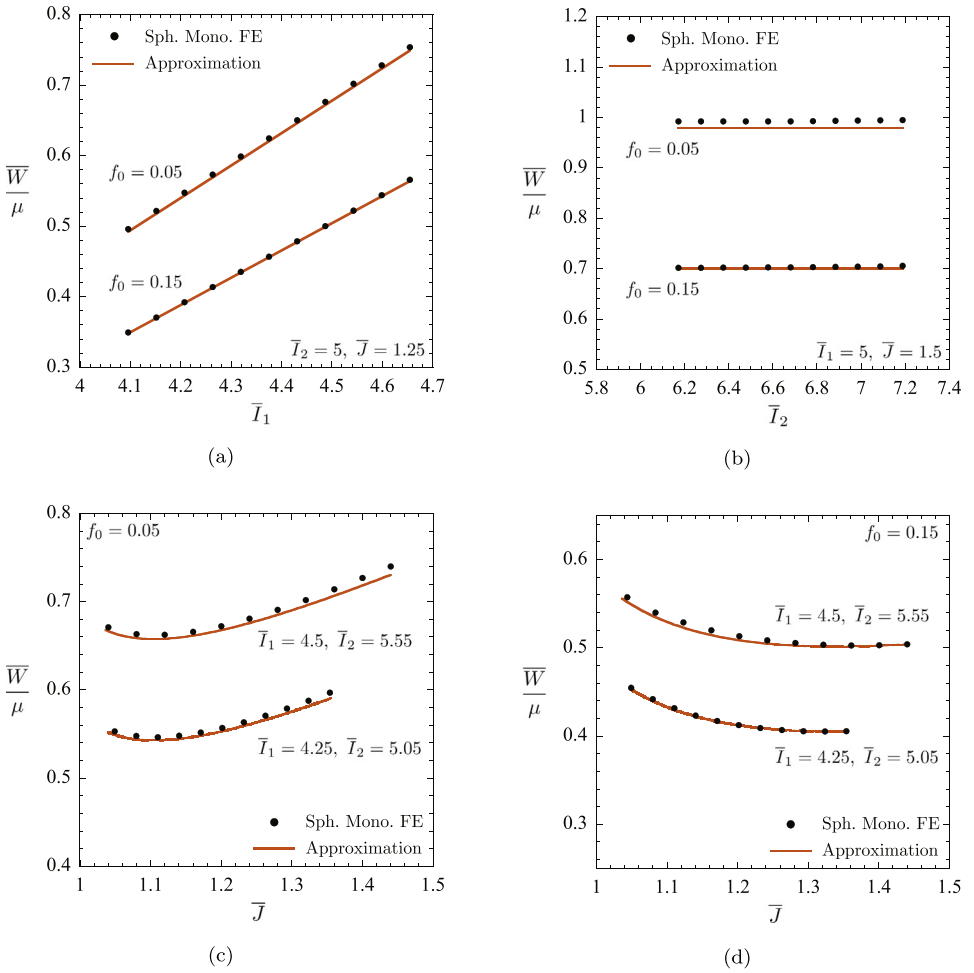

Fig. 7. The effective stored-energy function $\overline{W}$ of a porous Neo-Hookean elastomer wherein the pores are monodisperse in size and spherical in shape plotted as a function of each of the three invariants $\bar{I}_1,\ \bar{I}_2,\ \bar{J}$ for fixed values of the remaining two invariants. The results are shown normalized with the initial shear modulus μ of the elastomeric matrix for two different initial porosities, $f_0 = 0.05$ and 0.15. The dashed lines (labeled "Sph. Mono. FE") correspond to the FE solutions, while the solid lines (labeled "Approximation") correspond to the proposed explicit approximation (15).

Neo–Hookean elastomer with infinitely polydisperse pores of abstract shape, depends roughly linearly on the invariant $\bar{I}_1$, is roughly independent of $\bar{I}_2$, depends nonlinearly on $\bar{J}$, and is also approximately of the separable form $\overline{W} = \overline{W}_{\bar{I}_1}(\bar{I}_1, f_0) + \overline{W}_{\bar{J}}(\bar{J}, f_0)$, irrespectively of the applied deformation. A large set of results beyond the representative ones reported here have confirmed that such a remarkable functional dependence on the invariants holds true irrespectively of the value of the initial porosity f_0 (at least up to the maximum value of $f_0 = 0.30$ that we considered in our simulations).

4. An explicit approximate solution for porous Neo-Hookean elastomers

We are now in a position to state the first main analytical result of this paper. Indeed, the close agreement in the limit of small deformations together with the common functional dependence on the macroscopic deformation gradient $\overline{\mathbf{F}}$ exhibited by the solutions presented above for four different classes of isotropic porous microstructures with equiaxed closed-cell vacuous pores prompts the following explicit approximate solution for the effective stored-energy function of porous Neo-Hookean elastomers with *any type of non-percolative isotropic distribution of equiaxed closed-cell vacuous pores*:

$$\overline{W}(\overline{\mathbf{F}}, f_0) = \frac{3(1-f_0)\mu}{2(3+2f_0)}\left[\bar{I}_1 - 3\right] + \frac{3\mu}{2\bar{J}^{1/3}}\left[2\bar{J} - 1 - \frac{(1-f_0)\bar{J}^{1/3}\left(3\bar{J}^{2/3} + 2f_0\right)}{3+2f_0} - \frac{f_0^{1/3}\bar{J}^{1/3}\left(2\bar{J} + f_0 - 2\right)}{\left(\bar{J} - 1 + f_0\right)^{1/3}}\right]. \tag{15}$$

By design, in the limit of small deformations, the effective stored-energy function (15) agrees identically with the exact result (11) for the porous Neo-Hookean elastomer with the iterative microstructure discussed in Section 2, wherein, once

more, the pores are infinitely polydisperse in size and of abstract shape. By the same token, as established by the results shown in Fig. 6, it also provides a very accurate approximation for porous Neo-Hookean elastomers containing spherical and non-spherical pores of the same or different size, at least from $f_0 = 0$ up to an initial porosity of $f_0 = 0.30$.

Also by design, for isotropic finite deformations, the stored-energy function (15) has the further merit to agree identically with the exact result (13) for porous Neo-Hookean elastomers with the iterative microstructure discussed in Section 2, as well as with the HSA microstructure of Hashin.

Finally, for arbitrary finite deformations, while not exact, the effective stored-energy function (15) is expected to remain accurate — qualitatively as well as quantitatively — given that, by design, it is linear in the invariant $\bar{I}_1$, independent of $\bar{I}_2$, nonlinear in $\bar{J}$, and of the separable form $\overline{W} = \overline{W}_{\bar{I}_1}(\bar{I}_1, f_0) + \overline{W}_{\bar{J}}(\bar{J}, f_0)$. The comparisons shown above in Figs. 1 and 7 and further below in Fig. 8 support this expectation.

5. An explicit approximate solution for porous non-Gaussian elastomers

Next, we make use of the nonlinear comparison medium method[8] introduced in Lopez-Pamies et al. (2013), together with the approximate solution (15) for the effective stored-energy function of porous Neo-Hookean elastomers to construct the main analytical result of this work, namely, the simple explicit approximate solution (5) announced in the Introduction for the effective stored-energy function $\overline{W}$ of porous non-Gaussian elastomers.

We begin by defining the local stored-energy function of a "comparison porous elastomer" with the same isotropic microstructure as the porous elastomer of interest, that is, with the same characteristic function θ_0 as in $(2)_2$, but possibly different elastomeric matrix:

$$V(\mathbf{F},\mathbf{X}) = [1-\theta_0(\mathbf{X})]V_{\rm m}(\mathbf{F}) \qquad \text{with} \qquad V_{\rm m}(\mathbf{F}) = \begin{cases} \phi_{\rm m}(I_1) & \text{if} \quad J=1 \\ +\infty & \text{otherwise} \end{cases}.$$

As elaborated in Section 4 of Lopez-Pamies et al. (2013), it follows that the effective stored-energy function $(3)_2$ of any porous non-Gaussian elastomer of interest can be approximated variationally directly in terms of the effective stored-energy function

$$\overline{V}(\bar{\mathbf{F}}, f_0) = \min_{\mathbf{F}\in\mathcal{K}} \int_{\Omega_0} V(\mathbf{X},\mathbf{F})\mathrm{d}\mathbf{X} \tag{16}$$

of the "comparison porous elastomer". The result reads formally as follows:

$$\overline{W}\big(\bar{\mathbf{F}}, f_0\big) = \begin{cases} \sup\limits_{\phi_{\rm m}} \left\{ \overline{V}(\bar{\mathbf{F}}, f_0) + (1-f_0) \min\limits_{\mathcal{J}_1} [\Psi_{\rm m}(\mathcal{J}_1) - \phi_{\rm m}(\mathcal{J}_1)] \right\} & \text{if} \quad \Psi_{\rm m} - \phi_{\rm m} > -\infty \\ \inf\limits_{\phi_{\rm m}} \left\{ \overline{V}(\bar{\mathbf{F}}, f_0) + (1-f_0) \max\limits_{\mathcal{J}_1} [\Psi_{\rm m}(\mathcal{J}_1) - \phi_{\rm m}(\mathcal{J}_1)] \right\} & \text{if} \quad \Psi_{\rm m} - \phi_{\rm m} < \infty \end{cases}. \tag{17}$$

Now, by choosing the elastomeric matrix in the "comparison porous elastomer" to be Neo-Hookean with $\phi_{\rm m} = \nu/2[I_1 - 3]$ and by approximating the resulting effective stored-energy function (16) with the result (15) established in the preceding section, it is straightforward to carry out the sup-min and the inf-max operations in (17) and to deduce in turn that the variational approximation (17) reduces in this case to the simple explicit expression

$$\overline{W}(\bar{\mathbf{F}}, f_0) = (1-f_0)\Psi_{\rm m}\left(\frac{\mathcal{I}_1}{1-f_0} + 3\right) \tag{18}$$

with

$$\mathcal{I}_1 = \frac{3(1-f_0)}{3+2f_0}\big[\bar{I}_1 - 3\big] + \frac{3}{\bar{J}^{1/3}}\left[2\bar{J} - 1 - \frac{(1-f_0)\bar{J}^{1/3}\left(3\bar{J}^{2/3} + 2f_0\right)}{3+2f_0} - \frac{f_0^{1/3}\bar{J}^{1/3}\left(2\bar{J} + f_0 - 2\right)}{\left(\bar{J} - 1 + f_0\right)^{1/3}}\right]. \tag{19}$$

The effective stored-energy function (18)–(19) constitutes the main analytical result of this paper. It characterizes the macroscopic elastic response of isotropic porous elastomers that are comprised of an isotropic incompressible non-Gaussian elastomer, with any stored-energy function (1) of choice, embedding any type of non-percolative isotropic distribution of equiaxed closed-cell vacuous pores with initial porosity f_0. The following remarks are in order:

Remark 1. *The macroscopic constitutive response.* The macroscopic constitutive relation $(3)_1$ implied by the effective stored-energy function (18)–(19) is given by the simple explicit expression

$$\bar{\mathbf{S}} = \frac{6(1-f_0)}{3+2f_0}\Psi'_{\rm m}\left(\frac{\mathcal{I}_1}{1-f_0} + 3\right)\bar{\mathbf{F}} + \left[\frac{3+6\bar{J}+2f_0(1+7\bar{J})}{(3+2f_0)\bar{J}^{1/3}} + \frac{f_0^{1/3}\bar{J}(4-5f_0-4\bar{J})}{(\bar{J}+f_0-1)^{4/3}}\right]\Psi'_{\rm m}\left(\frac{\mathcal{I}_1}{1-f_0} + 3\right)\bar{\mathbf{F}}^{-T}. \tag{20}$$

[8] The interested reader is referred to Sections 1 and 4 in Lopez-Pamies et al. (2013) for an account of the historical development of comparison medium methods, including a brief outline of several of the major contributions which are most relevant to the present work (deBotton and Shmuel, 2010; Ponte Castañeda, 1991; Talbot and Willis, 1985; Willis, 1991; 1994).

Remark 2. *The limit of small deformations.* In the limit of small deformations as $\bar{\mathbf{F}} \to \mathbf{I}$, the effective stored-energy function (18)–(19) reduces asymptotically to

$$\overline{W}(\bar{\mathbf{F}}, f_0) = \widetilde{\mu}\,\mathrm{tr}\bar{\boldsymbol{\epsilon}}^2 + \left(\frac{\widetilde{\kappa}}{2} - \frac{\widetilde{\mu}}{3}\right)(\mathrm{tr}\bar{\boldsymbol{\epsilon}})^2 + O(||\bar{\mathbf{F}} - \mathbf{I}||^3),$$

where $\bar{\boldsymbol{\epsilon}} = (\bar{\mathbf{F}} + \bar{\mathbf{F}}^T - 2\mathbf{I})/2$ and where $\widetilde{\mu}$ and $\widetilde{\kappa}$ denote, again, the HS bounds (12). Thus, the proposed effective stored-energy function is exact in the limit of small deformations for porous elastomers with the iterative microstructure discussed in Section 2. Moreover, it is also exact in the limit of small isotropic deformations for porous elastomers with the HSA microstructure and, while not exact, as substantiated by Fig. 6, it is very accurate for small deformations of arbitrary type for porous elastomers containing spherical and non-spherical pores of the same or different size.

Remark 3. *Independence of $\overline{W}$ on the invariant $\bar{I}_2$.* For finite deformations, the effective stored-energy function (18)–(19) is not exact in general. The comparisons with FE simulations presented further below in the next section indicate that it does provide, however, an accurate approximation. In this regard, we remark in particular that the effective stored-energy function (18)–(19) is independent of the second principal invariant $\bar{I}_2$. The origin of this independence can be traced back to the first step of the derivation, when the weak but existent dependence on $\bar{I}_2$ of the response of porous Neo-Hookean elastomers (see Sections 2 and 3) was neglected in order to favor analytical tractability. The second step of the derivation outlined in this section, *id est*, the comparison medium procedure to account for non-Gaussian behavior, did not introduce any dependence on $\bar{I}_2$ either. The FE simulations presented in the next section indicate that this distinctive functional trait is indeed exhibited by the corresponding exact solutions.

Remark 4. *Closure of the pores.* The effective stored-energy function (18)–(19) features the following asymptotic behavior:

$$\overline{W}(\bar{\mathbf{F}}, f_0) \to +\infty \qquad \text{as} \qquad \bar{J} \to 1 - f_0.$$

This is the macroscopic manifestation of the fact that the *current* porosity in any porous elastomer with incompressible elastomeric matrix, given by the simple kinematical relation (see, e.g., Sections 2 and 4.1 in Lopez-Pamies et al. (2011a))

$$f = \frac{\bar{J} - 1}{\bar{J}} + \frac{f_0}{\bar{J}},$$

vanishes, that is, complete closure of the underlying pores ensues, whenever the determinant of the macroscopic deformation gradient $\bar{\mathbf{F}}$ reaches the critical value $\bar{J} = 1 - f_0$, at which point the porous elastomer behaves as an incompressible solid for loadings with any further volumetric compression.

Remark 5. *Cavitation instabilities.* In the limit of vanishingly small initial porosity as $f_0 \to 0+$, when the pores can be thought of as *point defects* featuring shape and spatial distribution but no volume, the effective stored-energy function (18)–(19) reduces asymptotically to

$$\overline{W}(\bar{\mathbf{F}}, f_0) = \Psi_{\mathrm{m}}\left(\bar{I}_1 + \frac{3(\bar{J} - 1)}{\bar{J}^{1/3}}\right) + O\left(f_0^{1/3}\right). \tag{21}$$

For isochoric deformations when $\bar{J} = 1$, the leading order term in (21) agrees identically with the stored-energy function (1) of the underlying elastomeric matrix. For non-isochoric deformations when $\bar{J} > 1$, on the other hand, the leading order term in (21) differs drastically from (1) in that it is *finite*. This is because under loading conditions with sufficiently large ratios of hydrostatic-to-shear stresses, the initially zero-volume pores can "cavitate" and grow elastically to occupy a finite volume within the elastomer.

As elaborated in the works of Lopez-Pamies (2009) and Lopez-Pamies et al. (2011a,b), the critical stresses at which such cavitation instabilities ensue can be readily determined from the asymptotic result (21). Precisely,

$$\bar{\mathbf{S}}_{cr} = \lim_{f_0 \to 0+} \frac{\partial \overline{W}}{\partial \bar{\mathbf{F}}}(\bar{\mathbf{F}}_{cr}, f_0) = 2\Psi_{\mathrm{m}}'\left(\bar{\mathbf{F}}_{cr} \cdot \bar{\mathbf{F}}_{cr}\right)\bar{\mathbf{F}}_{cr} + 3\Psi_{\mathrm{m}}'\left(\bar{\mathbf{F}}_{cr} \cdot \bar{\mathbf{F}}_{cr}\right)\bar{\mathbf{F}}_{cr}^{-T} \tag{22}$$

in terms of the corresponding critical macroscopic deformation gradients $\bar{\mathbf{F}}_{cr}$, which in this case — given the incompressibility of the underlying elastomeric matrix — stand for all macroscopic deformation gradients with $\det \bar{\mathbf{F}}_{cr} = 1$. For the special case of Neo-Hookean elastomers when $\Psi_{\mathrm{m}}' = \mu/2$, it is possible to rewrite the parametric form (22) of the loci of critical stresses in a simple implicit form. In terms of the principal stresses $\bar{t}_i$ of the Cauchy stress tensor $\bar{\mathbf{T}}_{cr} = \bar{\mathbf{S}}_{cr}\bar{\mathbf{F}}_{cr}^T$, the result reads as follows:

$$8\bar{t}_1\bar{t}_2\bar{t}_3 - 12\mu(\bar{t}_1\bar{t}_2 + \bar{t}_2\bar{t}_3 + \bar{t}_3\bar{t}_1) + 18\mu^2(\bar{t}_1 + \bar{t}_2 + \bar{t}_3) - 35\mu^3 = 0 \qquad \text{with} \qquad \bar{t}_i > \frac{3\mu}{2} \quad (i = 1, 2, 3),$$

which is nothing more than the onset-of-cavitation surface introduced in Lopez-Pamies et al. (2011b).

We close this remark by emphasizing that while the above-outlined phenomenon of cavitation instabilities within the theoretical context of elastostatics is mathematically sound (see, e.g., the celebrated paper by Ball, 1982), the phenomenon of "cavitation" found in actual elastomers appears to be a fracture phenomenon and *not* a purely elastic one (see, e.g., Kumar

et al., 2018; Lefèvre et al., 2015; Poulain et al., 2017). Thus, caution should be exercised in using the effective stored-energy function (18)–(19) to model the elastic response of porous elastomers with extremely small initial porosities f_0, as in such materials fracture might nucleate from the walls of the underlying pores at macroscopic deformations that are small.

Remark 6. *The case of porous Neo-Hookean elastomers.* For the basic case when the matrix is Neo-Hookean, namely, when, $\Psi_{\mathtt{m}} = \mu/2[I_1 - 3]$, the effective stored-energy function (18)–(19) reduces, of course, to the result (15) introduced in Section 4. The corresponding macroscopic constitutive relation (20) reduces in turn to

$$\overline{\mathbf{S}} = \frac{3(1-f_0)\mu}{3+2f_0}\,\overline{\mathbf{F}} + \frac{\mu}{2}\left[\frac{3+6\bar{J}+2f_0(1+7\bar{J})}{(3+2f_0)\bar{J}^{1/3}} + \frac{f_0^{1/3}\bar{J}(4-5f_0-4\bar{J})}{(\bar{J}+f_0-1)^{4/3}}\right]\overline{\mathbf{F}}^{-T}. \tag{23}$$

Remark 7. *Accounting for internal pore pressure.* Due to the fabrication process and/or environment of operation, the pores in closed-cell porous elastomers typically contain a gaseous substance that may exert a significant internal pressure on the surrounding elastomeric matrix. The formulation introduced in Idiart and Lopez-Pamies (2012) and Lopez-Pamies et al. (2012) allows one to directly transcribe the proposed macroscopic constitutive response (20) of a given porous elastomer with vacuous pores to the macroscopic constitutive response of the same porous elastomer when the underlying pores are pressurized internally.

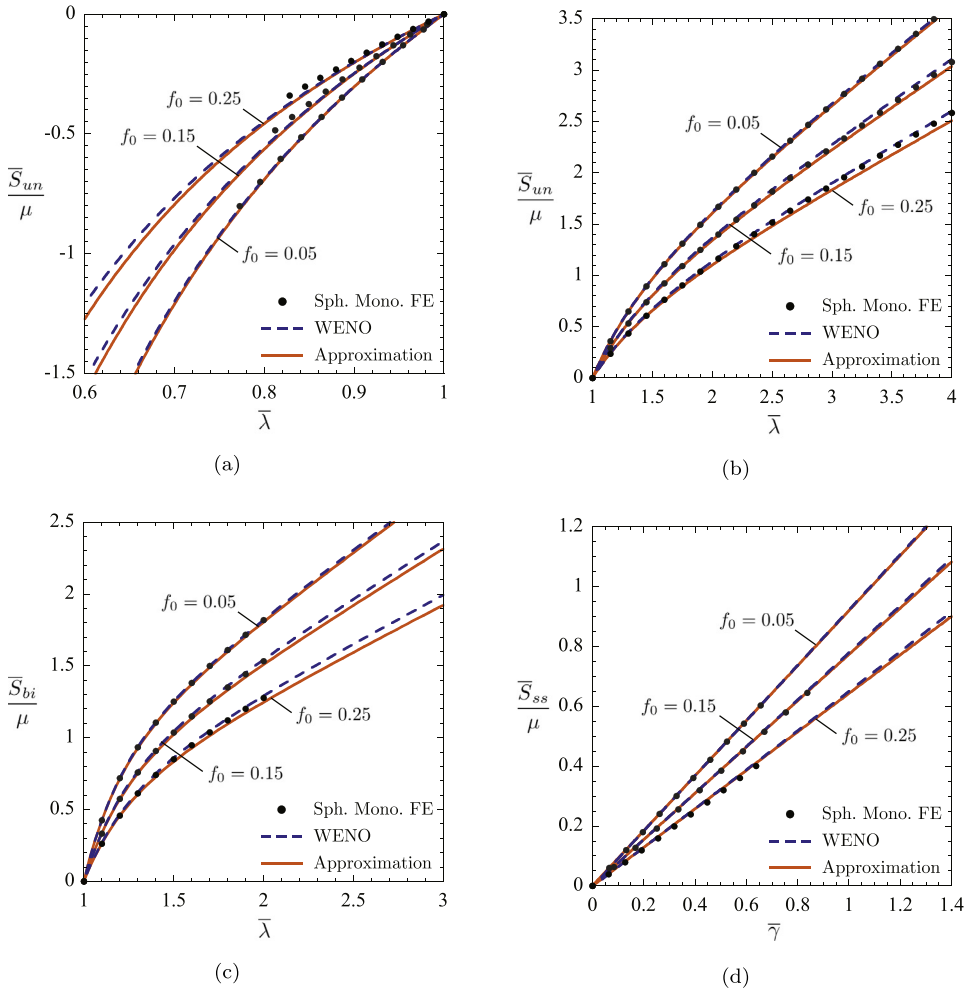

Fig. 8. Macroscopic response of porous Neo-Hookean elastomers with various values of initial porosity f_0 under: (a) uniaxial compression, (b) uniaxial tension, (c) biaxial tension, and (d) simple shear. Plots are shown for the appropriate component of the stress-deformation relation (23) — labeled "Approximation" and displayed as solid lines — together with corresponding WENO (dashed lines) and FE (solid circles) solutions for isotropic distributions of pores of infinitely polydisperse size and abstract shape and of monodisperse size and spherical shape.

6. Comparisons with WENO and FE solutions for porous Neo-Hookean and non-Gaussian elastomers

With the dual objective of further illustrating the accuracy of the proposed simple explicit homogenization solution for arbitrary finite deformations and of placing on record accurate computational solutions for a range of basic loading conditions, we close by confronting the general macroscopic stress-deformation response (20) to corresponding WENO and FE solutions for porous Neo-Hookean and non-Gaussian elastomers with the four classes of microstructures discussed in Sections 2 and 3. In particular, denoting by $\{\mathbf{e}_1, \mathbf{e}_2, \mathbf{e}_3\}$ the axes of the laboratory frame of reference, for possible direct connection with experiments, we present comparisons for the following four types of loading conditions that are accessible by standard experimental techniques:

- Uniaxial compression when $\overline{\mathbf{F}} = \overline{\lambda}\mathbf{e}_1 \otimes \mathbf{e}_1 + \overline{\lambda}_{lat}(\mathbf{e}_2 \otimes \mathbf{e}_2 + \mathbf{e}_3 \otimes \mathbf{e}_3)$ with $\overline{\mathbf{S}} = \overline{S}_{un}\mathbf{e}_1 \otimes \mathbf{e}_1$ and prescribed $\overline{\lambda} < 1$;
- Uniaxial tension when $\overline{\mathbf{F}} = \overline{\lambda}\mathbf{e}_1 \otimes \mathbf{e}_1 + \overline{\lambda}_{lat}(\mathbf{e}_2 \otimes \mathbf{e}_2 + \mathbf{e}_3 \otimes \mathbf{e}_3)$ with $\overline{\mathbf{S}} = \overline{S}_{un}\mathbf{e}_1 \otimes \mathbf{e}_1$ and prescribed $\overline{\lambda} > 1$;
- Biaxial tension when $\overline{\mathbf{F}} = \overline{\lambda}_{lat}\mathbf{e}_1 \otimes \mathbf{e}_1 + \overline{\lambda}(\mathbf{e}_2 \otimes \mathbf{e}_2 + \mathbf{e}_3 \otimes \mathbf{e}_3)$ with $\overline{\mathbf{S}} = \overline{S}_{bi}(\mathbf{e}_2 \otimes \mathbf{e}_2 + \mathbf{e}_3 \otimes \mathbf{e}_3)$ and prescribed $\overline{\lambda} > 1$; and
- Simple shear when $\overline{\mathbf{F}} = \mathbf{e}_1 \otimes \mathbf{e}_1 + \mathbf{e}_2 \otimes \mathbf{e}_2 + \mathbf{e}_3 \otimes \mathbf{e}_3 + \overline{\gamma}\mathbf{e}_1 \otimes \mathbf{e}_2$ with $\overline{\mathbf{S}} = \overline{S}_{ss}(\mathbf{e}_1 \otimes \mathbf{e}_2 + \mathbf{e}_2 \otimes \mathbf{e}_1)$ and prescribed $\overline{\gamma} > 0$.

We begin by presenting results for porous Neo-Hookean elastomers. Fig. 8 shows plots of the macroscopic stress-deformation response for the above outlined four types of loading conditions and three values of initial porosity, $f_0 = 0.05$, 0.15, and 0.25. The solid lines correspond to the appropriate component of the Neo-Hookean specialization (23) of the general result (20). On the other hand, the dashed lines and solid circles correspond to WENO and FE results for porous Neo-Hookean elastomers wherein, as discussed in Sections 2 and 3.2, the pores are infinitely polydisperse in size and of abstract shape and monodisperse in size and of spherical shape. We note that the FE results were computed up to the

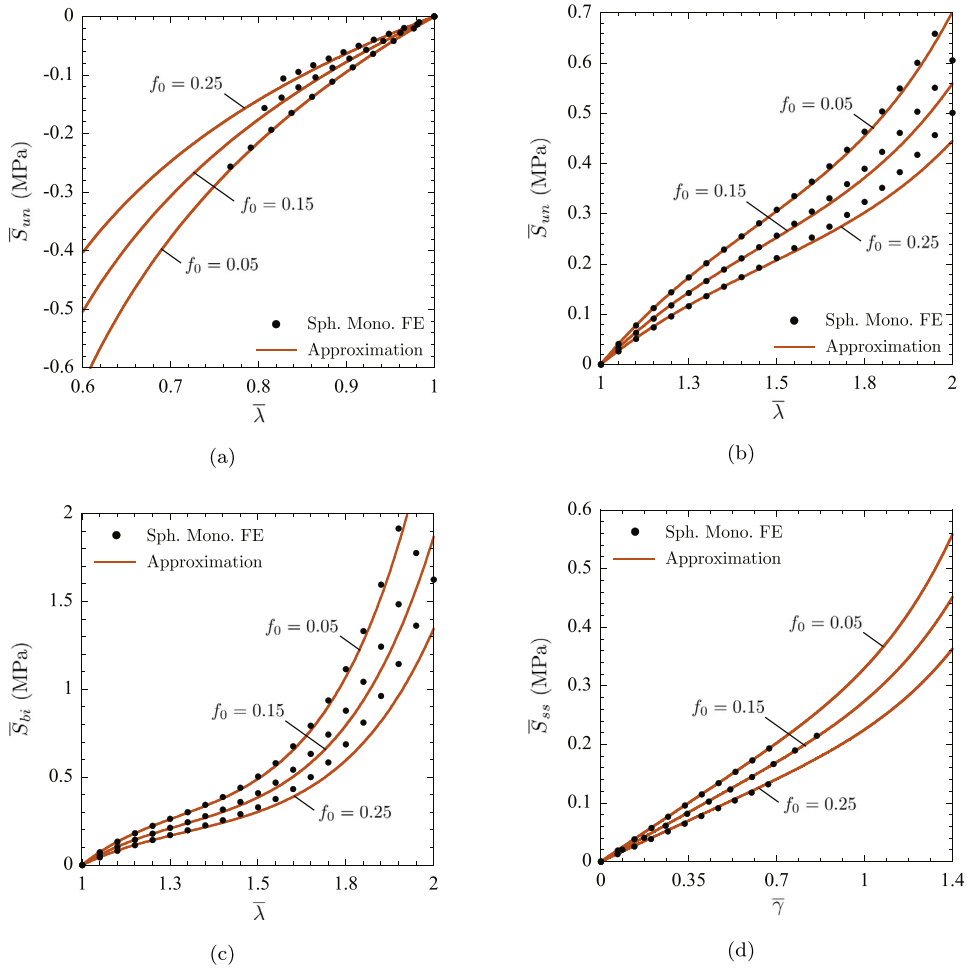

Fig. 9. Macroscopic response of porous silicone elastomers with various values of initial porosity f_0 under: (a) uniaxial compression, (b) uniaxial tension, (c) biaxial tension, and (d) simple shear. Plots are shown for the appropriate component of the stress-deformation relation (24) — labeled "Approximation" and displayed as solid lines — together with corresponding FE solutions (solid circles) for isotropic distributions of pores of monodisperse size and spherical shape.

point at which we managed to have a converged solution. More critically, we further note that, as it was the case for the effective stored-energy function $\overline{W}$ itself, the corresponding FE stress-deformation results for the isotropic distributions of polydisperse spherical pores and monodisperse oblate spheroidal pores described in Sections 3.1 and 3.3 are virtually indistinguishable from those presented in Fig. 8 for monodisperse spherical pores.

A quick glance at Fig. 8 suffices to recognize that the proposed macroscopic constitutive response (23) is in good agreement with both the WENO and the FE solutions for all loadings and all values of initial porosity considered. We should also mention that, for the cases of uniaxial and biaxial loading, the corresponding lateral stretches $\overline{\lambda}_{lat}$ implied by the constitutive response (23) are in equally good agreement with the lateral stretches obtained from the WENO and FE solutions.

Save for the exclusion of the WENO results, Fig. 9 shows analogous results to those shown in Fig. 8 for porous elastomers for which the constitutive behavior of the elastomeric matrix is characterized by the stored-energy function (Lopez-Pamies, 2010a)

$$W_{\rm m}(\mathbf{F}) = \begin{cases} \Psi_{\rm m}(I_1) = \sum_{r=1}^{2} \dfrac{3^{1-\alpha_r}}{2\alpha_r}\mu_r[I_1^{\alpha_r} - 3^{\alpha_r}] & \text{if} \quad J = 1 \\ +\infty & \text{otherwise} \end{cases}$$

with material parameters $\mu_1 = 0.26915$ MPa, $\mu_2 = 0.04406$ MPa, $\alpha_1 = 0.22743$, $\alpha_2 = 4.53944$. This particular choice of $W_{\rm m}$ happens to describe the non-Gaussian response of a commercial silicone elastomer of popular use; see Section 3 in Poulain et al. (2017). For this type of elastomeric matrix, it is a simple matter to work out that the macroscopic constitutive relation (20) specializes to

$$\begin{aligned} \overline{\mathbf{S}} = {} & \frac{1-f_0}{3+2f_0}\sum_{r=1}^{2} 3^{2-\alpha_r}\mu_r\left(\frac{\mathcal{I}_1}{1-f_0}+3\right)^{\alpha_r-1}\overline{\mathbf{F}} \\ & + \sum_{r=1}^{2} 3^{1-\alpha_r}\mu_r\left(\frac{\mathcal{I}_1}{1-f_0}+3\right)^{\alpha_r-1}\left[\frac{3+6\bar{J}+2f_0(1+7\bar{J})}{2(3+2f_0)\bar{J}^{1/3}} + \frac{f_0^{1/3}\bar{J}(4-5f_0-4\bar{J})}{2(\bar{J}+f_0-1)^{4/3}}\right]\overline{\mathbf{F}}^{-T}, \end{aligned} \tag{24}$$

where we recall that $\mathcal{I}_1$ is given by relation (19).

Much like the FE results in Fig. 8 for Neo-Hookean porous elastomers, we remark that the FE results in Fig. 9 for porous non-Gaussian elastomers with monodisperse spherical pores are essentially identical to their counterparts with polydisperse spherical and monodisperse oblate spheroidal pores. It is also apparent from Fig. 9 that the macroscopic constitutive response (24) is in fairly good agreement in this case too with the FE solutions, overall more so for smaller values of the initial porosity f_0.

Acknowledgments

Support for this work by the National Science Foundation through the Grant CMMI–1661853 is gratefully acknowledged. Part of this work was performed while V.L. was the Hibbitt Engineering Fellow at Brown University. Support from this fellowship is gratefully acknowledged.

Appendix A. The coefficients $\mathcal{G}_0$ through $\mathcal{G}_9$

The ten coefficients $\mathcal{G}_0$ through $\mathcal{G}_9$ entering the Hamilton–Jacobi Eq. (9) are given by

$$\mathcal{G}_0 = -\frac{3}{2} + \frac{1}{3}(\overline{\lambda}_1^2+\overline{\lambda}_2^2+\overline{\lambda}_3^2) + \frac{\Gamma_F}{2\overline{\lambda}_1\overline{\lambda}_2\overline{\lambda}_3^2},$$

$$\mathcal{G}_1 = \frac{\Gamma_E\overline{\lambda}_1\left(\overline{\lambda}_3^2-\overline{\lambda}_2^2\right)}{\overline{\lambda}_3\left(\overline{\lambda}_1^2-\overline{\lambda}_2^2\right)\left(\overline{\lambda}_1^2-\overline{\lambda}_3^2\right)} - \frac{\Gamma_F\overline{\lambda}_1}{\overline{\lambda}_1^2\overline{\lambda}_3-\overline{\lambda}_3^3} + \frac{\overline{\lambda}_2}{\overline{\lambda}_1^2\overline{\lambda}_3-\overline{\lambda}_2^2\overline{\lambda}_3} + \frac{\overline{\lambda}_1}{3},$$

$$\mathcal{G}_2 = \frac{\overline{\lambda}_2}{3} - \frac{\overline{\lambda}_1-\Gamma_E\overline{\lambda}_2}{\overline{\lambda}_1^2\overline{\lambda}_3-\overline{\lambda}_2^2\overline{\lambda}_3},$$

$$\mathcal{G}_3 = \frac{3(\Gamma_F-\Gamma_E)+\overline{\lambda}_1^2\overline{\lambda}_3-\overline{\lambda}_3^3}{3\left(\overline{\lambda}_1^2-\overline{\lambda}_3^2\right)},$$

$$\mathcal{G}_4 = \frac{\overline{\lambda}_1\overline{\lambda}_2\left(-\Gamma_E\overline{\lambda}_1\overline{\lambda}_2\left(\overline{\lambda}_1^2+\overline{\lambda}_2^2-2\overline{\lambda}_3^2\right)+\Gamma_F\overline{\lambda}_1\overline{\lambda}_2\left(\overline{\lambda}_2^2-\overline{\lambda}_1^2\right)+\left(\overline{\lambda}_1^2+\overline{\lambda}_2^2\right)\left(\overline{\lambda}_1^2-\overline{\lambda}_3^2\right)\right)}{3(\overline{\lambda}_1-\overline{\lambda}_2)^2(\overline{\lambda}_1+\overline{\lambda}_2)^2(\overline{\lambda}_1^2-\overline{\lambda}_3^2)},$$

$$\mathcal{G}_5 = \frac{\bar{\lambda}_1\bar{\lambda}_2\bar{\lambda}_3\left(\Gamma_E\bar{\lambda}_1\left(\bar{\lambda}_1^2-2\bar{\lambda}_2^2+\bar{\lambda}_3^2\right)+2\Gamma_F\bar{\lambda}_1\left(\bar{\lambda}_2^2-\bar{\lambda}_1^2\right)+\bar{\lambda}_2\left(\bar{\lambda}_1^2-\bar{\lambda}_3^2\right)\right)}{3\left(\bar{\lambda}_1^2-\bar{\lambda}_2^2\right)\left(\bar{\lambda}_1^2-\bar{\lambda}_3^2\right)^2},$$

$$\mathcal{G}_6 = -\frac{\bar{\lambda}_1\bar{\lambda}_2\bar{\lambda}_3\left(\Gamma_E\bar{\lambda}_2\left(-2\bar{\lambda}_1^2+\bar{\lambda}_2^2+\bar{\lambda}_3^2\right)+\Gamma_F\bar{\lambda}_2\left(\bar{\lambda}_1^2-\bar{\lambda}_2^2\right)+\bar{\lambda}_1\left(\bar{\lambda}_1^2-\bar{\lambda}_3^2\right)\right)}{3\left(\bar{\lambda}_1^2-\bar{\lambda}_2^2\right)\left(\bar{\lambda}_1^2-\bar{\lambda}_3^2\right)\left(\bar{\lambda}_2^2-\bar{\lambda}_3^2\right)},$$

$$\mathcal{G}_7 = -\frac{\bar{\lambda}_1^2\left(\bar{\lambda}_1^4-\bar{\lambda}_3^2\left(\bar{\lambda}_1^2+\bar{\lambda}_2^2\right)+2\bar{\lambda}_1^2\bar{\lambda}_2^2-\bar{\lambda}_2^4\right)}{6\left(\bar{\lambda}_1^2-\bar{\lambda}_2^2\right)^2\left(\bar{\lambda}_1^2-\bar{\lambda}_3^2\right)} - \frac{\Gamma_E\bar{\lambda}_1^3\bar{\lambda}_2\left(\bar{\lambda}_2^2-\bar{\lambda}_3^2\right)\left(-2\bar{\lambda}_1^2+\bar{\lambda}_2^2+\bar{\lambda}_3^2\right)}{3\left(\bar{\lambda}_1^2-\bar{\lambda}_2^2\right)^2\left(\bar{\lambda}_1^2-\bar{\lambda}_3^2\right)^2}$$
$$- \frac{\Gamma_F\bar{\lambda}_1^3\bar{\lambda}_2\left(-3\bar{\lambda}_1^2+2\bar{\lambda}_2^2+\bar{\lambda}_3^2\right)}{6\left(\bar{\lambda}_1^2-\bar{\lambda}_2^2\right)\left(\bar{\lambda}_1^2-\bar{\lambda}_3^2\right)^2},$$

$$\mathcal{G}_8 = \frac{\bar{\lambda}_2^2\left(-2\Gamma_E\bar{\lambda}_1\bar{\lambda}_2\left(\bar{\lambda}_1^2-2\bar{\lambda}_2^2+\bar{\lambda}_3^2\right)+\Gamma_F\bar{\lambda}_1\bar{\lambda}_2\left(\bar{\lambda}_1^2-\bar{\lambda}_2^2\right)+\bar{\lambda}_1^4+\bar{\lambda}_3^2\left(\bar{\lambda}_1^2+\bar{\lambda}_2^2\right)-2\bar{\lambda}_1^2\bar{\lambda}_2^2-\bar{\lambda}_2^4\right)}{6\left(\bar{\lambda}_1^2-\bar{\lambda}_2^2\right)^2\left(\bar{\lambda}_2^2-\bar{\lambda}_3^2\right)},$$

$$\mathcal{G}_9 = \frac{\bar{\lambda}_3^2\left(-2\Gamma_E\bar{\lambda}_1\bar{\lambda}_2\left(\bar{\lambda}_1^2+\bar{\lambda}_2^2-2\bar{\lambda}_3^2\right)+\Gamma_F\bar{\lambda}_1\bar{\lambda}_2\left(\bar{\lambda}_1^2+2\bar{\lambda}_2^2-3\bar{\lambda}_3^2\right)+\left(\bar{\lambda}_1^2-\bar{\lambda}_3^2\right)\left(\bar{\lambda}_1^2+\bar{\lambda}_2^2-\bar{\lambda}_3^2\right)\right)}{6\left(\bar{\lambda}_1^2-\bar{\lambda}_3^2\right)^2\left(\bar{\lambda}_2^2-\bar{\lambda}_3^2\right)}. \tag{25}$$

In the above expressions,

$$\Gamma_F = \frac{\bar{\lambda}_3}{\sqrt{\bar{\lambda}_3^2-\bar{\lambda}_2^2}}\mathcal{E}_F\left\{\frac{\sqrt{\bar{\lambda}_3^2-\bar{\lambda}_2^2}}{2\sqrt{\bar{\lambda}_2^2-\bar{\lambda}_3^2}}\ln\left[\frac{2\bar{\lambda}_2\left(\bar{\lambda}_2+\sqrt{\bar{\lambda}_2^2-\bar{\lambda}_3^2}\right)}{\bar{\lambda}_3^2}-1\right];\frac{\bar{\lambda}_1^2-\bar{\lambda}_3^2}{\bar{\lambda}_2^2-\bar{\lambda}_3^2}\right\},$$

$$\Gamma_E = \frac{\bar{\lambda}_3}{\sqrt{\bar{\lambda}_3^2-\bar{\lambda}_2^2}}\mathcal{E}_E\left\{\frac{\sqrt{\bar{\lambda}_3^2-\bar{\lambda}_2^2}}{2\sqrt{\bar{\lambda}_2^2-\bar{\lambda}_3^2}}\ln\left[\frac{2\bar{\lambda}_2\left(\bar{\lambda}_2+\sqrt{\bar{\lambda}_2^2-\bar{\lambda}_3^2}\right)}{\bar{\lambda}_3^2}-1\right];\frac{\bar{\lambda}_1^2-\bar{\lambda}_3^2}{\bar{\lambda}_2^2-\bar{\lambda}_3^2}\right\},$$

where the functions $\mathcal{E}_F$ and $\mathcal{E}_E$ stand for, respectively, the incomplete elliptic integrals of first and second kind, as defined by

$$\mathcal{E}_F\{\varphi;k\} = \int_0^\varphi [1-k\sin^2\theta]^{-1/2}\mathrm{d}\theta \qquad \text{and} \qquad \mathcal{E}_E\{\varphi;k\} = \int_0^\varphi [1-k\sin^2\theta]^{1/2}\mathrm{d}\theta.$$

Supplementary material

Supplementary material associated with this article can be found, in the online version, at doi:10.1016/j.jmps.2018.09.026.

References

ABAQUS Version 6.14 Documentation, 2014a. Dassault Systemes Simulia Corp., Providence, RI, USA.

Anoukou, K., Brenner, R., Hong, F., Pellerin, M., Danas, K., 2018. Random distribution of polydisperse ellipsoidal inclusions and homogenization estimates for porous elastic materials. Comput. Struct. doi:10.1016/j.compstruc.2018.08.006.

Avellaneda, M., 1987. Iterated homogenization, differential effective medium theory and applications. Commun. Pure Appl. Math. 40, 527–554.

Ball, J.M., 1982. Discontinuous equilibrium solutions and cavitation in nonlinear elasticity. Philos. Trans. R. Soc. A 306, 557–611.

Boffi, D., Brezzi, F., Fortin, M., 2013. Mixed Finite Element Methods and Applications. Springer, New York.

Danielsson, M., Parks, D.M., Boyce, M.C., 2004. Constitutive modeling of porous hyperelastic materials. Mech. Mater. 36, 347–358.

deBotton, G., 2005. Transversely isotropic sequentially laminated composites in finite elasticity. J. Mech. Phys. Solids 53, 1334–1361.

deBotton, G., Shmuel, G., 2010. A new variational estimate for the effective response of hyperelastic composites. J. Mech. Phys. Solids 58, 466–483.

Donev, A., Cisse, I., Sachs, D., Variano, E.A., Stillinger, F.H., Connelly, R., Torquato, S., Chaikin, P.M., 2004. Improving the density of jammed disordered packings using ellipsoids. Science 203, 990–993.

Francfort, G.A., Murat, F., 1986. Homogenization and optimal bounds in linear elasticity. Arch. Ration. Mech. Anal. 94, 307–334.

Gusev, A.A., 1997. Representative volume element size for elastic composites: a numerical study. J. Mech. Phys. Solids 45, 1449–1459.

Hashin, Z., 1985. Large isotropic elastic deformation of composites and porous media. Int. J. Solids Struct. 21, 711–720.

Hashin, Z., Shtrikman, S., 1963. A variational approach to the theory of the elastic behaviour of multiphase materials. J. Mech. Phys. Solids 11, 127–140.

Hill, R., 1972. On constitutive macrovariables for heterogeneous solids at finite strain. Proc. R. Soc. Lond. A 326, 131–147.

Hou, H.S., Abeyaratne, R., 1992. Cavitation in elastic and elasticplastic solids. J. Mech. Phys. Solids 40, 571–592.
Idiart, M.I., 2008. Modeling the macroscopic behavior of two-phase nonlinear composites by infinite-rank laminates. J. Mech. Phys. Solids 56, 2599–2617.
Idiart, M.I., Lopez-Pamies, O., 2012. On the overall response of elastomeric solids with pressurized cavities. Comptes Rendus Mecanique 340, 359–368.
Kumar, A., Francfort, G.A., Lopez-Pamies, O., 2018. Fracture and healing of elastomers: A phase-transition theory and numerical implementation. J. Mech. Phys. Solids 112, 523–551.
Lefèvre, V., Garnica, A., Lopez-Pamies, O., 2018. A WENO finite-difference scheme for a new class of Hamilton–Jacobi equations in nonlinear solid mechanics. In preparation.
Lefèvre, V., Lopez-Pamies, O., 2014. The overall elastic dielectric properties of a suspension of spherical particles in rubber: An exact explicit solution in the small-deformation limit. J. Appl. Phys. 116, 134106.
Lefèvre, V., Lopez-Pamies, O., 2017. Nonlinear electroelastic deformations of dielectric elastomer composites: I — Ideal elastic dielectrics. J. Mech. Phys. Solids 99, 438–470.
Lefèvre, V., Ravi-Chandar, K., Lopez-Pamies, O., 2015. Cavitation in rubber: an elastic instability or a fracture phenomenon? Int. J. Fract. 192, 1–23.
Lopez-Pamies, O., 2009. Onset of cavitation in compressible, isotropic, hyperelastic solids. J. Elast. 94, 115–145.
Lopez-Pamies, O., 2010a. A new I_1-based hyperelastic model for rubber elastic materials. Comptes Rendus Mecanique 338, 3–11.
Lopez-Pamies, O., 2010b. An exact result for the macroscopic response of particle-reinforced Neo-Hookean solids. J. Appl. Mech. 77, 021016.
Lopez-Pamies, O., Goudarzi, T., Danas, D., 2013. The nonlinear elastic response of suspensions of rigid inclusions in rubber: II — A simple explicit approximation for finite-concentration suspensions. J. Mech. Phys. Solids 61, 19–37.
Lopez-Pamies, O., Idiart, M.I., 2009. An exact result for the macroscopic behavior of porous Neo-Hookean solids. J. Elast. 95, 99–105.
Lopez-Pamies, O., Idiart, M.I., Nakamura, T., 2011a. Cavitation in elastomeric solids: I — A defect-growth theory. J. Mech. Phys. Solids 59, 1464–1487.
Lopez-Pamies, O., Nakamura, T., Idiart, M.I., 2011b. Cavitation in elastomeric solids: II — Onset-of-cavitation surfaces for Neo-Hookean materials. J. Mech. Phys. Solids 59, 1488–1505.
Lopez-Pamies, O., Ponte Castañeda, P., 2004. Second-order estimates for the macroscopic response and loss of ellipticity of porous rubbers at large deformations. J. Elast. 76, 247–287.
Lopez-Pamies, O., Ponte Castañeda, P., 2007a. Homogenization-based constitutive models for porous elastomers and implications for macroscopic instabilities: I — Analysis. J. Mech. Phys. Solids 55, 1677–1701.
Lopez-Pamies, O., Ponte Castañeda, P., 2007b. Homogenization-based constitutive models for porous elastomers and implications for macroscopic instabilities: II — Results. J. Mech. Phys. Solids 55, 1702–1728.
Lopez-Pamies, O., Ponte Castañeda, P., Idiart, M.I., 2012. Effects of internal pore pressure on closed-cell elastomeric foams. Int. J. Solids Struct. 49, 2793–2798.
MATLAB Version 8.3 Documentation, 2014b. Mathworks, Natick, Massachusetts, USA.
Michel, J.C., Lopez-Pamies, O., Ponte Castañeda, P., Triantafyllidis, N., 2007. Microscopic and macroscopic instabilities in finitely strained porous elastomers. J. Mech. Phys. Solids 55, 900–938.
Michel, J.C., Moulinec, H., Suquet, P., 1999. Effective properties of composite materials with periodic microstructure: a computational approach. Comput. Methods Appl. Mech. Eng. 172, 109–143.
Milton, G.W., 2002. The Theory of Composites. Cambridge University Press.
Moraleda, J., Segurado, J., Llorca, J., 2007. Finite deformation of porous elastomers: a computational micromechanics approach. Philos. Mag. 87, 5607–5627.
Ogden, R.W., 1978. Extremum principles in non-linear elasticity and their application to composites. I. Theory. Int. J. Solids Struct. 14, 265–282.
Ponte Castañeda, P., 1991. The effective mechanical properties of nonlinear isotropic composites. J. Mech. Phys. Solids 39, 45–71.
Poulain, X., Lefèvre, V., Lopez-Pamies, O., Ravi-Chandar, K., 2017. Damage in elastomers: Nucleation and growth of cavities, micro-cracks, and macro-cracks. Int. J. Fract. 205, 1–21.
Schöbel, J., 1997. Netgen an advancing front 2d/3d-mesh generator based on abstract rules. Comput. Visual. Sci. 1, 41–52.
Segurado, J., Llorca, J., 2002. A numerical approximation to the elastic properties of sphere-reinforced composites. J. Mech. Phys. Solids 50, 2107–2121.
Shu, C.W., 2009. High order weighted essentially nonoscillatory schemes for convection dominated problems. SIAM Rev. 51, 82–126.
Spinelli, S.A., Lefèvre, V., Lopez-Pamies, O., 2015. Dielectric elastomer composites: A general closed-form solution in the small-deformation limit. J. Mech. Phys. Solids 83, 263–284.
Talbot, D.R.S., Willis, J.R., 1985. Variational principles for inhomogeneous nonlinear media. IMA J. Appl. Math. 35, 39–54.
Wang, Y., Henann, D.L., 2016. Finite-element modeling of soft solids with liquid inclusions. Extrem. Mech. Lett. 9, 147–157.
Williams, S.R., Philipse, A.P., 2003. Random packings of spheres and spherocylinders simulated by mechanical contraction. Phys. Rev. E 67, 051301.
Willis, J.R., 1991. On methods for bounding the overall properties of nonlinear composites. J. Mech. Phys. Solids 338, 3–11.
Willis, J.R., 1994. Upper and lower bounds for the properties of nonlinear composites. Mater. Sci. Eng. A 175, 7–14.
Zee, L., Sternberg, E., 1983. Ordinary and strong ellipticity in the equilibrium theory of incompressible hyperelastic solids. Arch. Ration. Mech. Anal. 83, 53–90.